2010

Simulation of condensation in a circular minichannel: Application of VOF method and turbulence model

Enrico Da Riva
University of Padova

David Del Col
University of Padova

Alberto Cavallini
University of Padova

Suresh Garimella
CTRC, sureshg@purdue.edu

Simulation of condensation in a circular minichannel: Application of VOF method and turbulence model

Enrico DA RIVA[1]*, Davide DEL COL[1], Alberto CAVALLINI[1], Suresh V. GARIMELLA[2]

[1]University of Padova, Dipartimento di Fisica Tecnica,
Via Venezia 1, I-35131 Padova, Italy
(Tel.: +390498276885, fax: +390498276896, enrico.dariva@unipd.it)

[2]Cooling Technologies Research Center, School of Mechanical Engineering,
Purdue University, 585 Purdue Mall, West Lafayette, IN 47907-2088, USA
(Tel.: +17654945621, sureshg@purdue.edu)

* Corresponding Author

ABSTRACT

Three-dimensional steady-state simulations of condensation of R134a in a horizontal minichannel are presented. Mass fluxes ranging from G = 100 kg m^{-2}s^{-1} up to G = 800 kg m^{-2}s^{-1} are considered in a circular minichannel of 1 mm inner diameter. The Volume of Fluid (VOF) method is used to track the vapour-liquid interface, with the effects of interfacial shear stress, gravity and surface tension taken into account. Uniform wall and vapour-liquid interface temperatures are imposed as boundary conditions. A low-Reynolds number form of the SST k-ω model (Menter, 1994) is used for turbulence modeling in both the liquid and vapour phases. The numerical results are compared against experimental data from Matkovic *et al.* (2009), as well as to simulations obtained by assuming laminar liquid film flow. The present numerical model is able to capture the influence of mass flux on the condensation heat transfer coefficient as obtained in experimental measurements.

1. INTRODUCTION

A more complete understanding and theoretical modeling of the two-phase flow and heat transfer process in minichannels is needed for the design and optimization of heat exchangers.

A theoretical study of film condensation in minichannels, taking into account surface tension, gravity and vapour shear stress was reported in Wang and Rose (2006). In their work, the condensate film is treated assuming laminar flow and neglecting inertia and convection terms. Moreover, different channel shapes were compared.

A number of different methods are currently available for the direct simulation of multiphase flows. These techniques can be very useful, in particular when trying to extend the investigation to new minichannel geometries. Simulations are presented in this paper using the Volume of Fluid (VOF) method which can handle multiphase flows of immiscible fluids, tracking the motion of the interface between them without using empirical closure laws to model the interaction between the phases. The capability of this method to take into account the surface tension force, in particular, is very promising, since the effect of surface tension is expected to be important at small scales and when using non-circular minichannel shapes.

A VOF simulation of condensation of R134a in a circular 1 mm minichannel at mass flux G = 200 kg m^{-2}s^{-1} was reported in Da Riva and Del Col (2009). Laminar flow was assumed for the liquid and turbulent flow for the vapour, and turbulence was handled by a low-Reynolds number form of the standard k-ω model (Wilcox, 1998), which was modified in order to suppress the turbulent viscosity inside the liquid phase. In the present work, the assumption of laminar flow for the condensate film is relaxed and a low-Re form of the SST k-ω model (Menter, 1994) is used for turbulence modeling throughout the computational domain. The efficacy of this simulation approach is assessed by comparing the numerical results with experimental data obtained at different mass fluxes.

Table 1: Cases considered in the simulations.

Mass Flux [kg m^{-2}s^{-1}]	**Re$_{GO}$** [-]	**Re$_{LO}$** [-]	**Channel Length** [mm]	**Outlet Quality** [-]
100	8,082	619	75	0.30
200	16,164	1,239	100	0.36
400	32,328	2,478	130	0.40
800	64,657	4,955	150	0.45

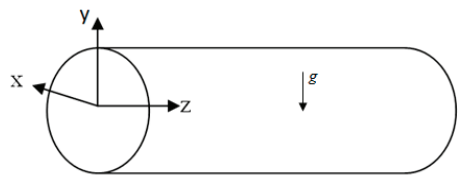

Fig. 1 Cartesian axis convection.

2. NUMERICAL SIMULATIONS

Three-dimensional steady-state simulation of condensation of R134a in a 1 mm i.d. circular minichannel are performed at different mass fluxes (G = 100 kg m^{-2}s^{-1} to 800 kg m^{-2}s^{-1}). The inlet thermodynamic vapour quality is x = 1 and the channel is horizontally oriented. Both the effects of gravity and surface tension are taken into account. The simulations employ the VOF method implemented in the commercial code FLUENT 6.3 (Fluent, 2006). The minichannel wall is held isothermal at a uniform temperature of T_W = 30°C, while the saturation temperature of the fluid is T_S = 40°C. A pressure boundary condition is imposed at the outlet.

The Cartesian axis convention used is shown in Fig. 1. Details of the channel length, outlet vapour quality and all-liquid and all-vapour Reynolds numbers are reported in Table 1 for each case considered. It is noticed that the steady-state simulations performed in this work do not allow for intermittent flows such as plug/slug flows to be predicted. According to the flow pattern map for R134a in a 1 mm i.d. pipe developed from experimental visualizations at 52°C by Coleman and Garimella (2000), for the vapour quality range considered in Table 1, at G = 800 kg m^{-2}s^{-1}, "mist flow" is expected for x > 0.7 and "annular film and mist flow" is expected for x < 0.7; at G = 400 kg m^{-2}s^{-1} "annular film and mist flow" is expected along all the channel length; at G = 200 kg m^{-2}s^{-1}, "annular film flow" is expected for x > 0.5 and "plug/slug and annular film flow" is expected for x <0.5; finally, at G = 100 kg m^{-2}s^{-1}, "annular film flow" is expected for x > 0.8 and "plug/slug and annular film flow" is expected for x <0.8.

The domain is discretized into approximately 850,000 hexahedral cells. In order to fully resolve the liquid film region, the radial thickness of the cells in the near-wall region is ≈2 μm, while the mesh is much coarser in the core region. The axial length of the cells is around 100 μm.

Selected single-phase simulations are performed over a channel length of 1 m (i.e. 1000 times the hydraulic diameter) in order to obtain the fully developed turbulent solution for the vapour flow. The results of these simulations are then used to set the inlet boundary conditions for the z-velocity, the turbulent kinetic energy and the turbulent specific dissipation rate.

2.1 VOF Method

In the VOF method, the volume fraction α, representing the portion of the volume of the computational cell filled with one phase is tracked. The volume fractions of all phases sum to unity. The VOF algorithm is divided into two parts: a reconstruction step and a propagation step. The problem of interface reconstruction is that of finding an approximation to the section of the interface in each cut cell by knowing the volume fraction in that cell and in the neighbouring ones. Once the interface has been reconstructed, its motion due to the underlying flow field is modeled by an advection algorithm. The two-phase mixture is considered as a single fluid with properties changing depending on the value of the volume fraction α. Properties are computed for each cell as an arithmetic mean:

$$\varphi = \varphi_L \alpha_L + \varphi_G (1 - \alpha_L) \tag{1}$$

with $\varphi = \rho, \lambda, \mu$ ...

All properties are considered to be temperature-dependent and computed from the REFPROP8 database (NIST, 2007).

The following continuity equations are solved:

$$\nabla \cdot (\vec{u}\alpha_L) = \frac{S}{\rho_L} \tag{2}$$

$$\nabla \cdot (\vec{u}\alpha_G) = -\frac{S}{\rho_G} \tag{3}$$

where S is the mass source term due to phase change.
The usual Navier-Stokes equations are solved for momentum in the cells where only one of the two phases is present. At the interface (i.e. $0<\alpha_L<1$), the force due to the surface tension F_σ must be taken into account as:

$$\nabla \cdot (\rho\vec{u}\vec{u}) = -\nabla p + \nabla \cdot [(\mu + \mu_t)(\nabla\vec{u} + \nabla\vec{u}^T)] + \rho\vec{g} + \vec{F}_\sigma \tag{4}$$

The effect of surface tension is written in terms of a pressure jump across the interface. The volume force due to the surface tension is computed by means of the Continuum Surface Force (CSF) model proposed by Brackbill *et al.* (1992), as follows:

$$\kappa_L = \nabla \cdot \frac{\nabla\alpha_L}{|\nabla\alpha_L|} \tag{5}$$

$$\vec{F}_\sigma = \sigma_{LG} \frac{\rho\kappa_L\nabla\alpha_L}{0.5(\rho_L + \rho_G)} \tag{6}$$

where κ is the surface curvature and σ_{LG} is the surface tension.
All scalar values are shared by the phases throughout the domain, and thus no particular special treatment is needed for the energy or turbulence equations.
The following energy equation is solved:

$$\nabla \cdot (\vec{u}\rho h) = \nabla \cdot (\lambda_{eff}\nabla T) + h_{LV}S \tag{7}$$

where λ_{eff} is the effective thermal conductivity, h is the specific enthalpy and the last term (i.e. $h_{LV}\,S$) is the energy source due to phase change. The specific enthalpy is computed as follows:

$$h = \frac{\alpha_L\rho_L h_L + \alpha_G\rho_G h_G}{\alpha_L\rho_L + \alpha_G\rho_G} \qquad h(T) = \int_{298.15}^{T} c_p\, dT + h^0(298.15) \tag{8}$$

where $h^0(298.15)$ is the standard state enthalpy at 298.15 K.
The low-Re form of the SST k-ω model (Menter, 1994) used for turbulence modeling displays a gradual change from the standard k-ω model in the inner region of the boundary layer to a high-Reynolds version of the k-ε model in the outer part of the boundary layer. Besides, as compared to the standard k-ω model, a modified formulation of the turbulent viscosity is adopted in order to take into account the transport effects of the principal turbulent shear stress. The Green-Gauss node-based method (Holmes and Connell, 1989) is used for evaluation of gradients. An implicit time discretization along with the modified High Resolution Interface Capturing (HRIC) scheme (Muzaferija *et al.*, 1998) is used for VOF calculations. Pressure interpolation is conducted with the PRESTO! scheme while pressure-velocity coupling is accomplished by means of the SIMPLE algorithm. The third-order MUSCL scheme (Val Leer, 1979) is used for the momentum equation, the two turbulence equations and the energy equation.

2.2 Phase Change Modelling

The following equation can be used in order to estimate the interfacial heat transfer coefficient due to molecular kinetics effects (Berman, 1967, McNaught and Butterworth, 1994):

$$h_i = 0.53\frac{p\,h_{LV}^2\,M^{1.5}}{T_S^{2.5}R^{1.5}} \tag{9}$$

More recently, the following equation has been proposed in the literature (Wang and Rose, 2004):

$$h_i = 2.66 \frac{\gamma_G - 1}{\gamma_G + 1} \frac{\rho_G \, h_{LV}^2 \, M^{0.5}}{T_S^{1.5} R^{0.5}} \tag{10}$$

where γ_G is the ratio of specific heat capacities for the vapour phase.
The expected interfacial heat transfer coefficient for R134a at 40°C is approximately h_i = 11 10^6 $Wm^{-2}K^{-1}$ according to Eq. (9) and h_i = 9 10^6 $Wm^{-2}K^{-1}$ according to Eq. (10). Since the in-tube condensation heat transfer coefficient under the conditions considered in this work is lower than 25 10^3 $Wm^{-2}K^{-1}$, the molecular kinetic thermal resistance at the interface is negligible and the interfacial temperature can be assumed to be the saturation temperature.
The numerical technique described by Lee (1980) is employed in the simulations in order to model the phase-change process, and is given by:

$$\begin{aligned} S &= -r\alpha_L \rho_L \frac{T - T_S}{T_S} \qquad T \geq T_S \\ S &= r\alpha_G \rho_G \frac{T_S - T}{T_S} \qquad T < T_S \end{aligned} \tag{11}$$

where S is the source term in the continuity equations (2) and (3) and in the energy equation (7), T is the cell temperature and r is a positive numerical coefficient. If at some step of the computation, the temperature of a cell in the domain is higher than the saturation temperature, the first of the two equations is used: if this cell belongs to the vapour phase (i.e. $\alpha_L = 0$) no mass transfer is computed; if this cell belongs to the liquid phase (i.e. $\alpha_L > 0$), mass transfer from the liquid to the vapour phase is computed. Besides, the temperature of the cell is decreased by the source term due to phase change in the energy equation. The computation is analogous for the cells with temperature lower than the saturation temperature. In this way, the presence of cells in the vapour phase with temperature lower than the saturation temperature, as well as the presence of cells in the liquid phase with temperature higher than the saturation temperature is avoided. The source term S in Eq. (11) is arbitrarily fixed; however, mass, momentum and energy are conserved at every computational step.
At convergence, the interface should reach the saturation temperature, while all cells belonging to the liquid phase should reach a lower temperature and all cells belonging to the vapour a higher temperature. In practice, the interfacial temperature obtained by the use of this numerical technique will not be exactly the saturation temperature. Excessively small values of the coefficient r lead to a significant deviation between interfacial and saturation temperature. Furthermore, when higher values of the coefficient r are used, the interface (i.e. the region of cells with $0<\alpha_L<1$) is sharper and thinner. However, too large values of r cause numerical convergence problems and optimal values must be found for each case. In the present simulations, the coefficient r ranged from 1 10^6 to 2 10^7 and the deviation between interface and saturation temperatures was approximately 0.5 K.

3. RESULTS AND DISCUSSION

3.1 Comparison with laminar liquid film approach

A simulation of condensation inside a circular minichannel was presented in Da Riva and Del Col (2009) for the condensation of R134a at G = 200 kg $m^{-2}s^{-1}$. In this previous version of the present model, it was assumed that all along the channel the flow was laminar inside the entire liquid film and turbulent inside the vapour phase; a modified low-Re k-ω model (Wilcox, 1998) was adopted to model turbulence. In particular, the usual computation of the turbulent viscosity was modified as follows (Da Riva and Del Col, 2009):

$$\mu_t = f_1 \frac{\rho_G \, k}{\omega} \alpha_G \tag{12}$$

where f_1 is a dumping function for low-Re correction.
The turbulent viscosity μ_t given by Eq. (12) is zero along the channel wall in the entire condensate liquid film; therefore the turbulence production inside the liquid phase is suppressed and laminar flow is imposed. It is noted that the assumption of a laminar liquid film is common in the theoretical models to predict film condensation available in the literature (e.g. Wang and Rose, 2006, Nebuloni and Thome, 2010).

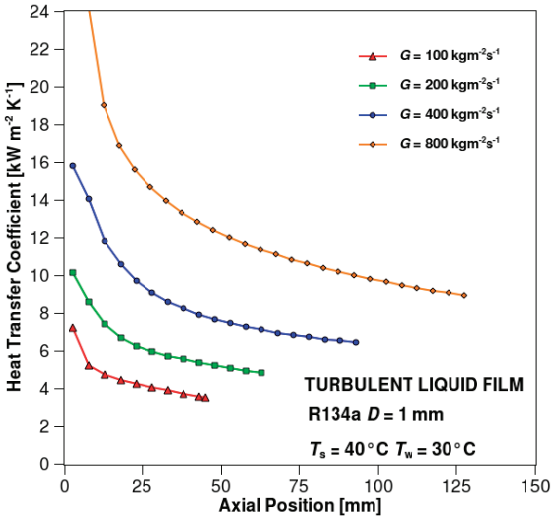

Fig. 2: Heat transfer coefficient as a function of axial position for the turbulent film approach. Each curve ends at $x = 0.5$.

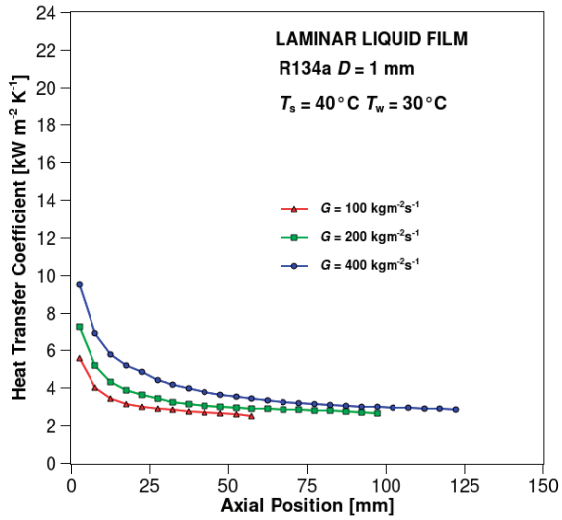

Fig. 3: Heat transfer coefficient as a function of axial position for the laminar film approach.

In the present simulations, a low Reynolds form of the SST k-ω model (Menter, 1994) was used for turbulence modeling throughout the entire computational domain without any modification, as described earlier. This semi-empirical model (as well as all models available for CFD) has been developed for single-phase flows; therefore its applicability across a gas-liquid interface has not been established. However, low-Reynolds forms of k-ω turbulence models should allow for the viscous sublayer and the laminar-turbulent transition to be resolved.

Heat transfer coefficients computed according to the present turbulence modeling approach and the laminar liquid film approach are plotted with respect to axial position in Fig. 2 and Fig. 3. All series reported in Fig. 2 end at x = 0.50.The two modeling approaches are seen to provide very different results, especially at high mass fluxes.

Axial velocities along the vertical axis at x = 0.75 for both turbulence modeling approaches considered in this section are compared in Fig. 4. Dots in the graph represent the position of the vapour-liquid interface. Again, it is clear that the two approaches yield different results. In the case of the laminar film approach, the velocity profile is linear across the entire condensate film, while in the other case a deviation from the linear profile due to the effect of turbulence can be seen, especially at the bottom of the minichannel.The most important difference, however, is due to the stratification of the condensate, which is much higher in the case of the laminar liquid film approach, which explains the much lower heat transfer coefficients predicted.

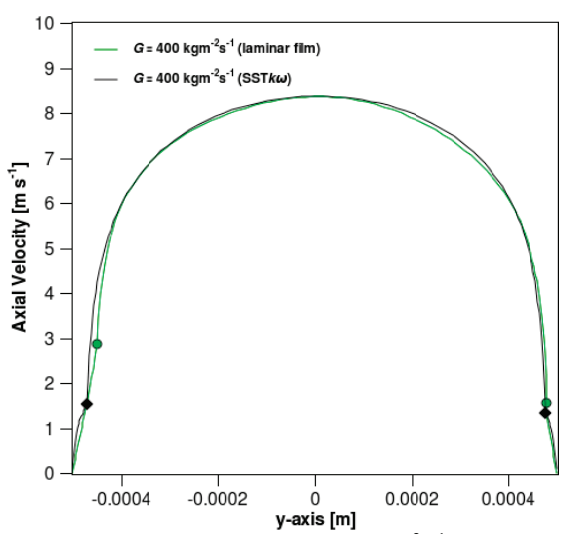

Fig. 4: Axial velocity along the vertical axis at $x = 0.75$, $G = 400$ kg m^{-2}s^{-1}. Present simulations and simulations based on the laminar film approach are compared.

The computed liquid film thickness at the top of the channel is approximately 20~25 μm in both cases, while at the bottom of the channel it is approximately 30 μm when the low-Re SST *k-ω* model is used for the condensate film, and 50 μm when the laminar film approach is used.

3.2 Comparison with experimental data (Matkovic *et al.*, 2009)

Cross-sectional average heat transfer coefficient computed according to the present turbulence modeling approach and the laminar liquid film approach are compared against experimental data from Matkovic *et al.* (2009) in Fig. 5 and Fig. 6, respectively. Experimental data were obtained in a 0.96 mm i.d. circular minichannel at the same saturation temperature as is considered in the present simulation. In the experimental apparatus used by Matkovic *et al.* (2009), R134a is cooled with water, which does not ensure that the saturation to wall temperature difference is constant all along the test section. For the experimental data reported in Fig. 5 and Fig. 6, this temperature difference ranges from T_s-T_w = 7.1 K up to T_s-T_w = 13.1 K, while in the simulations both the saturation and wall temperatures are constant and uniform all along the computational domain and the difference is T_s-T_w = 10 K.

The experimental measurements for R134a at G = 417 kg m^{-2}s^{-1} and for R32 at G = 200 kg m^{-2}s^{-1} displayed no effect of the saturation to wall temperature difference on the condensation heat transfer coefficient. Since no effect of this temperature difference is expected down to G = 200 kg m^{-2}s^{-1}, experimental and computational results can be directly compared, provided that the heat transfer coefficient is plotted versus the thermodynamic vapour quality.

As seen in Fig. 6, in the case of the laminar liquid film approach, the mass flux displays a very weak influence on the heat transfer coefficient only at high vapour qualities, while for vapor qualities less than x = 0.8, the three series overlap. Such behavior is not consistent with the experimental data. For the simulations performed adopting the low-Re SST *k-ω* model for the condensate film, instead, a strong influence of the mass flux can be seen in Fig. 5.

The numerical results obtained by means of the turbulent film approach presented in this work overpredict experimental data at low mass fluxes, but show good agreement at high mass fluxes with a maximum absolute error of 21% at G = 400 kg m^{-2}s^{-1} and 10% at G = 800 kg m^{-2}s^{-1}. In contrast the laminar film approach overpredicts experimental data at high mass fluxes, but shows reasonable agreement at G = 100 kg m^{-2}s^{-1} with a maximum absolute error of 15%.

An analysis of the velocity field provides interesting insights into the predictions from the present model. The predicted axial velocity profiles along the vertical axis (i.e. y-axis, see Fig. 1) at vapour quality x = 1 down to x = 0.4 are reported in Fig. 7 and Fig. 8 for G = 200 kg m^{-2}s^{-1} and G = 400 kg m^{-2}s^{-1}, respectively. The diamond-shaped symbols in the graph represent the position of the vapour-liquid interface. As the vapour quality is decreased, the film thickness stays almost constant at the top of the minichannel, while it gets thicker at the bottom, since some of the liquid condensed in the upper part of the tube is drained to the bottom by gravity.

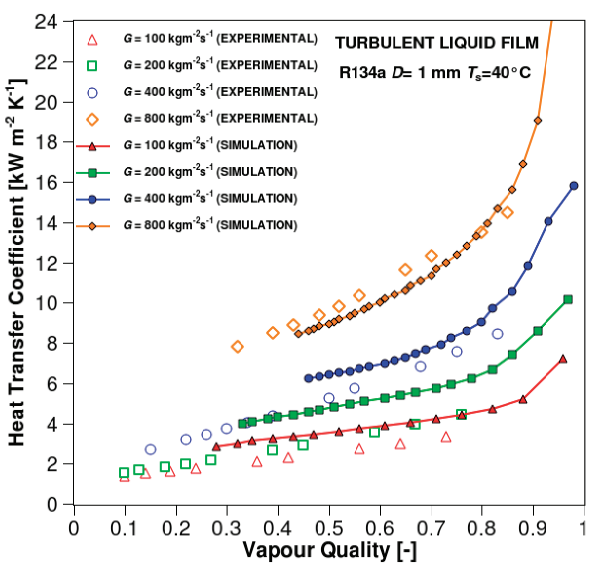

Fig. 5: Heat transfer coefficient as a function of vapour quality. Simulations with turbulent liquid film approach and experimental data from Matkovic *et al*. (2009).

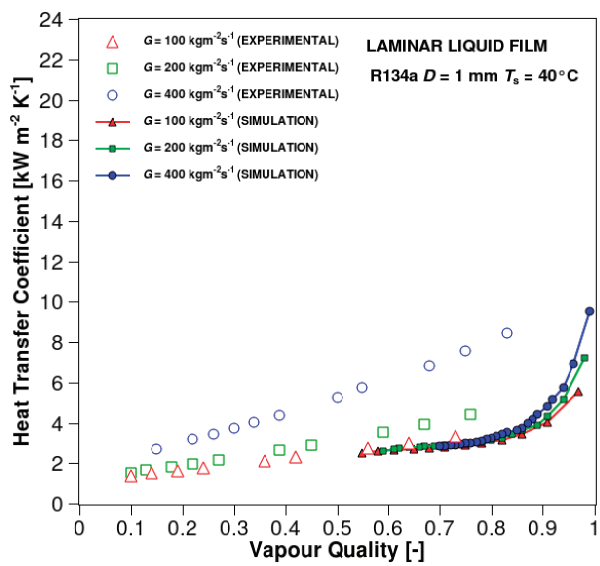

Fig. 6: Heat transfer coefficient as a function of vapour quality. Simulations with laminar liquid film approach and experimental data from Matkovic *et al*. (2009).

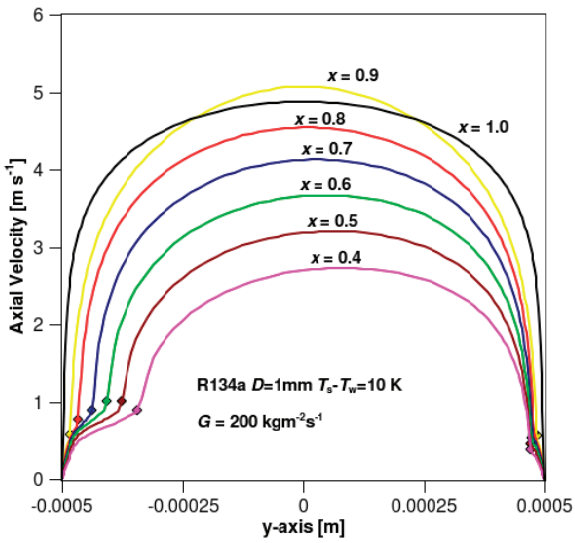

Fig. 7: Axial velocity along vertical axis at different vapour qualities and $G = 200$ kg m^{-2}s^{-1}.

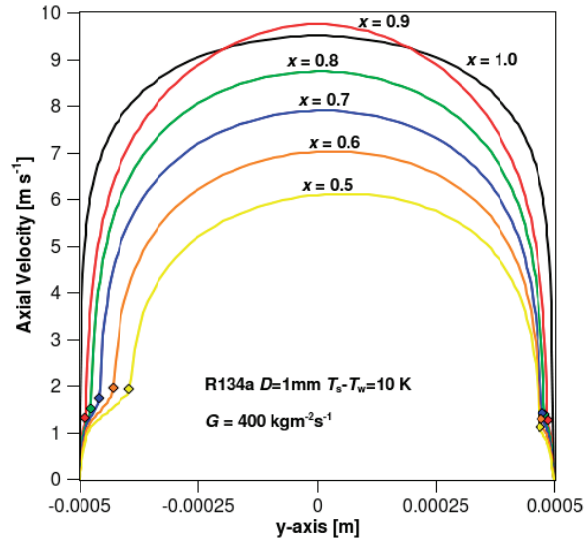

Fig. 8: Axial velocity along vertical axis at different vapour qualities and $G = 400$ kg m^{-2}s^{-1}.

At the beginning of the condensation process, the velocity profile is symmetrical and no effect of the stratification of liquid at the bottom of the tube is shown, but moving downstream the velocity profile becomes more and more asymmetrical and the mean velocity of the vapour phase decreases because of condensation.

4. CONCLUSIONS

Three-dimensional steady-state simulations of condensation of R134a in a 1 mm diameter horizontal circular minichannel are presented. The VOF method is used to track the vapour-liquid interface and both the effects of gravity and surface tension are taken into account.

A low-Re form of the SST k-ω model (Menter, 1994) is used for turbulence modeling in both liquid and vapour phases. This modeling approach is compared against the hypothesis of laminar condensate film flow as well as experimental data from Matkovic *et al.* (2009).

Numerical results obtained by means of the laminar condensate film approach predict experimental data at the lowest mass flux (i.e. $G = 100$ kg m^{-2}s^{-1}) with 15% maximum deviation, but fail to capture the influence of the mass flux on the condensation heat transfer coefficient seen in experimental measurements. When plotting the heat transfer coefficient versus vapour quality, some weak influence is predicted only at high vapour qualities.

The low-Re turbulence modeling of the condensate film proposed in the present work, instead, overpredicts the experimental data at low mass fluxes, but captures the influence of the mass flux and predict experimental data at $G = 400$ kg m^{-2}s^{-1} with 21% maximum deviation and experimental data at $G = 800$ kg m^{-2}s^{-1} with 10% maximum deviation.

NOMENCLATURE

A	cross sectional area $\pi D^2/4$	(m^2)
c_p	isobaric specific heat	(J kg^{-1}K^{-1})
c_v	isochoric specific heat	(J kg^{-1}K^{-1})
D	internal diameter	(m)
g	gravity acceleration	(kg m s^{-2})
G	mass flux, m/A	(kg m^{-2}s^{-1})
h_{LV}	latent heat	(J kg^{-1})
m	mass flow rate	(kg s^{-1})
M	molar mass	(kg kmol^{-1})
p	pressure	(Pa)
R	universal gas constant	(JK^{-1}kmol^{-1})

Subscripts

eff	effective
G	gas/vapour phase
L	liquid phase
S	saturation
W	wall

Re_{GO}	all-vapour Reynolds GD/μ_G	(-)
Re_{LO}	all-liquid Reynolds $GD/\mu L$	(-)
S	phase change mass source	(kg m^{-3}s^{-1})
T	temperature	(K)
u	velocity	(ms^{-1})
x	thermodynamic vapour quality	(-)
Greek letters		
α	volume fraction	(-)
γ	ratio of specific heat capacities	$\gamma = c_p/c_v$ (-)
κ	interface curvature	(m^{-1})
λ	thermal conductivity	(Wm^{-1}K^{-1})
μ	dynamic viscosity	(Pa s)
ρ	density	(kg m^{-3})
σ	surface tension	(N m^{-1})

REFERENCES

Berman, L.D., 1967, On the effect of molecular kinetic resistance upon heat transfer with condensation, *IJHMT*, vol. 10, p. 1463, 1967.

Brackbill, J.U., Kothe D. B., Zemach, C., 1992, A Continuum Method for Modeling Surface Tension. *J. Comput. Phys.* 100, 335-354.

Coleman, J.W., Garimella, S., 2000, Two-phase flow regime transitions in microchannel tubes: the effect of hydraulic diameter, Orlando, FL: *American Society of Mechanical Engineers*, *Heat Transfer Division*, 71-83.

Da Riva, E., Del Col, D., 2009, Numerical simulation of condensation in a minichannel, *Proc. ASME 2009 2nd Micro/Nanoscale Heat & Mass Transfer International Conference*, December 18-22, 2009, Shanghai, China.

Fluent, 2006, Fluent 6.3 User`s Guide, Lebanon, NH, Fluent Inc.

Holmes, D.G. and Connell, S.D., 1989, Solution of the 2D Navier-Stokes Equations on Unstructured Adaptive Grids. *Proc. AIAA 9th Computational Fluid Dynamics Conference*, June 1989.

Lee, W.H., 1980, A pressure iteration scheme for two-phase flow modeling, in: T.N. Veziroglu (Ed.), Multiphase Transport Fundamentals, Reactor Safety, Applications, vol. 1, Hemisphere Publishing, Washington DC.

Matkovic, M., Cavallini, A., Del Col, D., Rossetto, L., 2009, Experimental study on condensation heat transfer inside a single circular minichannel, *IJHMT*, vol. 52, p. 2311-2323.

McNaught, J.M. and Butterworth, D., 1994, Film condensation of pure vapour – Interfacial (molecular kinetic) resistance, in *Heat Exchanger Design Handbook*, Begell House, p. 2.6.2-14.

Menter, F.R., 1994, Two-Equation Eddy-Viscosity Turbulence Models for Engineering Applications. *AIAA Journal*, 32(8), p. 1598-1605.

Muzaferija, S., Peric, M., Sames, P., Schellin, T., 1998, A two-fluid Navier-Stokes solver to simulate water entry. *Proc. 22nd Symposium on Naval Hydrodynamics*, 277-289, Washington DC.

Nebuloni, S., Thome, J.R., 2010, Numerical modeling of laminar annular film condensation for different channel shapes, *IJHMT*, vol. 53, 2615-2627.

NIST, 2007, National Institute of Standard and Technology, Refprop8, Boulder Colorado.

Van Leer, B., 1979. Toward the ultimate conservative difference scheme. IV. A second order sequel to Godunov's method. *Journal of Computational Physics*, vol. 32, 101-136.

Wang, H.S., Rose, J.W., 2004, Effect of interphase matter on condensation on low-finned tubes – a theorethical investigation, *IJHMT*, vol. 47, 179-184.

Wang, H.S., Rose, J.W., 2006, Film condensation in horizontal microchannels: Effect of channel shape, *International Journal of Thermal Science*, vol. 45, p. 1205-1212.

Wilcox, D.C., 1998, Turbulence Modeling for CFD. DCW Industries, Inc., La Canada, California, USA.